Electrocatalyst design for direct borohydride oxidation guided by first principles

Gholamreza Rostamikia,[a] Romesh J. Patel,[b] Irene Merino-Jimenez,[c] Michael Hickner,[b] and Michael J. Janik[a*]

a Department of Chemical Engineering, Pennsylvania State University, University Park, PA 16802
b Department of Materials Science and Engineering, Pennsylvania State University, University Park, PA 16802
c Bristol Robotics Laboratory, Universities of Bristol and of the West of England, Bristol Business Park, Coldharbour Lane, BS16 1QY, UK

Abstract

Density functional theory (DFT) calculations are used to propose a Au-Cu binary metal catalyst for the electrochemical borohydride oxidation reaction (BOR), which is evaluated experimentally and observed to show enhanced oxidation activity relative to a pure Au electrode. Our previous work has applied DFT methods to determine the BOR mechanism and elucidate the key reaction steps that dictate catalyst activity and selectivity to complete oxidation. A balanced initial adsorption strength of the borohydride anion is essential for an active and selective catalyst. Adsorption must be strong enough to provide a reasonable coverage of surface species and promote B-H bond dissociation but not so strong as to promote easy dissociation and provide a high coverage of surface H atoms that result in H_2 evolution. Borohydride adsorption energetics were evaluated for a series of close-packed pure metal surfaces. Copper catalysts appear encouraging, but are not electrochemically stable under reaction conditions. Gold-copper alloys are predicted to show increased activity compared to a pure gold electrode, while maintaining the selectivity to direct oxidation and increasing

the stability compared to pure Cu. DFT results suggest an approximately 0.2 V decrease in the overpotential for borohydride oxidation on a $Au_2Cu_1(111)$ electrode compared to a Au(111) electrode. This DFT predicted reduction in overpotential is realized experimentally. Electrodeposition was used to prepare AuCu electrodes and their borohydride oxidation electrokinetics were examined by linear sweep voltammetry. An 88.5% gold and 11.5% copper sample demonstrated an overpotential reduction of 0.17 V compared to a pure Au electrode. The binding energy and adsorption free energy of BH_4^- over other surface alloys is also examined to further identify promising BOR electrodes.

1. Introduction

Direct borohydride fuel cells (DBFC's) utilize a high energy density, aqueous borohydride solution to directly convert chemical energy to electrical energy. There are a number of advantages and disadvantages regarding use of these fuel cells as an alternative energy conversion device. The aqueous fuel used in DBFC's does not have the storage and handling concerns associated with hydrogen fuel cells and the final product is an environmentally benign product that may be recycled. In addition to the energy intensity of borohydride synthesis, the main challenge in developing DBFC's is the low efficiency of electrocatalysts used for the borohydride oxidation reaction (BOR). Previously tested materials, mainly noble metals, either suffer from low activity or low selectivity for the oxidation reaction, which limits the fuel cell efficiency to approximately 30%.

Multiple materials have been tested experimentally as anode electrocatalysts for DBFC's. Gold[1-5] and silver[3, 6] are more selective catalysts, which could produce up to 8

electrons per borohydride molecule, however, the low activity of these catalysts limit the fuel cell efficiency and high overpotentials are required to draw sizable currents from these catalysts. Platinum,[1, 7-8] nickel,[7-9] and palladium[7] are more active for borohydride oxidation reactions, however an extreme activity of these catalysts for breaking B-H bonds leads to large amounts of hydrogen gas production and less than 8 e⁻ collected per borohydride molecule converted.   This lack of selectivity also limits the overall efficiency of the fuel cell.

We have previously applied density functional theory (DFT) methods to evaluate the borohydride oxidation mechanism over the Au(111)[10-11] and Pt(111) surfaces,[12] as well as Pd-Ir alloys.[13] Our mechanistic studies[10-11] of the BOR over the Au(111) surface concluded that the unfavorable borohydride adsorption and low activity for breaking B-H bonds causes low activity and large overpotentials. Alternatively, very exothermic, dissociative adsorption of BH_4^- ions over the platinum surface produces a large surface coverage of hydrogen. Recombination of the surface hydrogen as hydrogen molecules, competes with the surface hydrogen oxidation which causes the unselective production of hydrogen gas over this surface.

There are a few experimental attempts to use alloy catalysts for direct borohydride anodes. In most cases a combination of more selective catalysts like gold and more active catalysts like platinum or palladium is used.[13-17] Non-noble metals such as Ni have also been considered for bimetallic alloys with Au. Ni would reduce the cost of the catalyst and keep or even improve the catalytic activity towards the borohydride oxidation.[18] A Pt-Dy alloy electrode was also tested for the BOR reaction.[19] Pt-Dy alloys show comparable current density to pure platinum at room temperature, however, they have a

higher coulombic efficiency than platinum at elevated temperatures. Chatenet et al. reviewed and compared the activity (power density and current density) of different alloys (AuPt, PtRu, NiPt, AgNi, AuNi, NiPd) to pure gold and platinum electrodes.[20] All these alloys are more active than gold electrodes, however, they also produce higher amount of hydrogen. Carbon supported palladium and copper nanoparticles were also considered for BOR and show better performance than pure palladium nanoparticles.[21] DFT studies were also performed on Pd-Ir alloys for BOR,[13] suggesting that the presence of Ir favored borohydride oxidation rather than the hydrogen evolution and increased the number of electrons released from the BOR when the concentration of Ir was increased.

Gold nanoparticles combined with amorphous Co-B (Au@Co-B) have been also considered for borohydride oxidation and the activity has been reported to be higher than pure gold electrodes.[22] These studies have concluded that alloy electrodes may increase the power density and improve the performance of the cell, increasing the current density and decreasing the overpotential, though the majority of these are not as selective to direct oxidation as pure Au electrodes.

Au alloyed with 3d metals have been shown to promote borohydride oxidation and retain selectivity to direct oxidation. He et al. carried out cyclic voltammetry, chronopotentiometry and chronoamperometry with different alloys composed by Au and 3d transition metals (M = Fe, Co, Ni, Cu and Zn).[23] Besides being a less expensive catalyst for borohydride oxidation, Au-M/C alloys have a higher specific activity for borohydride oxidation than pure Au, leading to a higher open circuit potential in the DBFC and more rapid borohydride oxidation. The authors assured that Au-Zn, Au-Fe and

Au-Cu showed no activity towards borohydride hydrolysis, minimizing one of the main problems of the DBFC.

Density functional theory (DFT) calculations can be used to predict the relative performance of various metal alloys for the BOR. As we have identified the adsorption free energy of BH_4^- ions to the electrode surface as a key indicator of electrocatalyst activity and selectivity, its evaluation with DFT can be used to predict catalyst performance. Weak molecular bonding of BH_4* (where "*" denotes a surface species) will lead to a more selective catalyst, however, the activity of such catalysts for breaking B-H bonds will limit the activity. Strong dissociative adsorption indicates a more active catalyst, however, facile B-H dissociation will lead to a non-selective catalyst producing H_2 gas as well as oxidation products. Moderate molecular adsorption of BH_4^- ions to the catalyst surface will produce the best efficiency for the BOR, balancing the activity of the catalyst while maintaining selectivity to complete oxidation.

In addition to our initial study of Au-Cu alloys for BOR, the Kasai group has applied DFT to examine Au-based bimetallic electrocatalysts.[24-25] Arevalo et al.[25] used first principles calculations based on spin-polarized DFT to study the adsorption of borohydride ions on Au and Au_3M (111) (M = Cr, Mn, Fe, Co and Ni). They obtained more favorable adsorption configurations and larger adsorption stability on the alloys than on pure Au. For all the alloys considered, the adsorption energy increased between 0.33 and 0.58 eV compared to that on pure Au. In the case of pure Au, when the sp state of borohydride hybridizes with the d band, both bonding and antibonding states are fully occupied. The occupied states near the Fermi level contribute to a repulsive interaction due to antibonding characteristics. In the case of the alloys, the derived sp-d state is

upshifted and becomes unoccupied unlike on pure Au. That explains the increase in the adsorption energy of borohydride on Au_3M surfaces compared to pure Au.

Herein, we apply DFT to examine a series of alloy surfaces, and present a more complete elementary borohydride oxidation path for a Au-Cu alloy that shows strong promise for increased activity while maintaining selectivity against hydrolysis. Similar to our previous mechanistic studies over the Au(111) and Pt(111) surfaces,[10, 12] we use a vacuum-slab DFT model to evaluate the initial electrochemical adsorption of BH_4^- ions to a series of late transition metal surfaces. Metal alloys with potentially improved BOR performance are chosen based on a rationale developed from the pure metal behavior. The selected alloys are investigated for their initial BH_4^- adsorption strength, and the complete oxidation energetics are evaluated for the especially promising Au-Cu catalyst. Experimental studies (electrodeposition, characterization, and voltammetry) realize the predicted enhanced activity of the Au-Cu catalyst.

2. Research methods

2.1. Computational methods

All calculations were performed using the ab initio total-energy and molecular-dynamics Vienna ab initio simulation program (VASP) developed at the Institute for Material Physics at the University of Vienna.[26-28] Interactions of ions and electrons were described by using projected augmented wave method.[29] Exchange and correlation energies were calculated using the Perdew-Wang form of generalized gradient approximation.[30] In all calculations, plane-wave basis sets were used with a cut off energy of 400 eV. A $3\times3\times1$ Monkhorst-Pack grid[31] was used for sampling the Brillouin

zone during optimization of structures, followed by a 4×4×1 single point calculation to give the total energy. A 5×5×1 Monkhorst-Pack grid[31] was used for sampling the Brillouin zone to search for the saddle points using the climbing image nudged elastic band method. To determine the zero point vibrational (ZPVE) corrections to the total energy of adsorbates, the harmonic vibrational modes were calculated.

Pure metal surfaces and the Au_2Cu_1 bimetallic were modeled using a 4 layer slab and a 3×3 surface cell. An experimental value of 3.94 Å was used as the lattice parameter of the Au_2Cu_1 fcc bimetallic structure.[32] Two bottom layers were constrained and the two top layers of the metal slabs were allowed to relax. 13 Å of vacuum was inserted between the periodic slabs. Adsorption of BH_4 species and borohydride oxidation intermediates were examined over the high symmetry atop, bridge, fcc and hcp sites. The energy of the adsorbed species were corrected for spurious slab-to-slab dipole interactions along the surface normal direction (VASP keywords LDIPOL=TRUE, IDIPOL=3).

Adsorption energies and the elementary surface reactions energetics were calculated using the lowest energy adsorbed states. Calculation of the adsorption energies and the elementary surface reaction energetics has been detailed in our previous publications.[10, 12]

2.2 Experimental methods

Electrodeposition experiments and linear sweep voltammetry (LSV) experiments were carried out using a computer controlled potentiostat (PARSTAT 2273, Princeton Applied Research). An aqueous solution of 1mM $HAuCl_4$, 2-5 mM $CuSO_4$ and 0.05 M H_2SO_4 was used for deposition of a Au-Cu alloy over a 5 mm platinum disk electrode at

7

constant potential (-0.045 V Ag/AgCl) for 1600 seconds. Prior to the deposition of the Au-Cu alloy, the platinum electrode was polished to a mirror finish using 1 μm and 0.05 μm alumina paste. The Pt electrode was chosen over a BOR-inert glassy carbon electrode because it offered more predictable electrodeposition kinetics and better adhesion of the deposited Au-Cu layer. Scanning electron microscopy (SEM, supplementary information) confirmed that the deposited thick layer did not leave any Pt exposed, and voltammetry studies showed no indication of borohydride oxidation or hydrogen evolution around -0.8 V(NHE) expected for a Pt electrode. Deposition and borohydride oxidation voltammetry experiments were performed in a standard three-electrode cell. An Ag/AgCl (4 M KCl) reference electrode was used in all experiments, and all reported potentials are shifted to reference a normal hydrogen electrode. All potentials given in the text are relative to a normal hydrogen electrode unless otherwise noted. A platinum wire was used as the counter electrode in deposition experiments. Alternatively, for linear sweep voltammetry (LSV) tests a graphite rod was used as a counter electrode. For LSV experiments, 0.03 M $NaBH_4$ and 2 M NaOH were used.

2-dimentional wide angle x-ray diffraction (2D-WAXD) was carried out using a Rigaku RAPID II x-ray generator diffractometer (Tokyo, Japan) with Ni-filtered Cu Kα radiation (λ = 1.54059Å) and a tube voltage and current of 50 KV and 40 mA. The incidence angle was rocked between 30° and 50° at a frequency of 1 s^{-1} for 1 hour and the resulting 2D WAXD patterns were integrated.

3. Results and discussion

A more effective electrocatalyst is designed for the borohydride oxidation guided by first-principles DFT calculations, and the recommended Au-Cu binary metal catalyst is tested experimentally to confirm the improved activity. The initial adsorption strength of the BH_4^- species is examined as a design parameter in section 3.1. As the $Au_2Cu_1(111)$ surface is encouraging based on this initial analysis, the complete oxidation mechanism is examined over this surface in section 3.2. The optimal binding configuration and energy of the surface reaction intermediates are reported in section 3.2.1. Elementary surface reaction energetics are presented and discussed in section 3.2.2. Experimental characterization and voltammetry realizing the predicted improvement in electrocatalytic activity for the Au-Cu catalyst are presented in section 3.3. In section 3.4, DFT methods are used to generate other potentially active and selective bimetallic surfaces.

3.1. Adsorption of BH_4^- ions over close-packed, late transition metal surfaces

The adsorption of the BH_4^- anion is taken to occur with electron transfer through the reaction:

$$BH_4^-{}_{(aq)} + H_2O* \rightarrow BH_4* + H_2O_{(aq)} + e^- \tag{1}$$

Adsorption of the borohydride ion is taken to displace a surface water molecule, which is returned to the aqueous phase upon desorption. As the adsorption reaction releases an electron, the adsorption free energy is dependent on the electrode potential. We calculate the adsorption free energy as a function of electrode potential as the difference in free energy between reactants and products in equation 1:

$$\Delta G_{ads}(U) = G_{BH_4*} + G_{H_2O_{aq}} - eU - G_{H_2O*} - G_{BH_4^-_{,aq}} \tag{2}$$

where a "*" denotes a surface species, U denotes the electrode potential on an absolute scale, and e^- is the absolute value of an elementary charge. We have previously detailed the methods used to approximate the solution phase chemical potential of the BH_4^- ion and an H_2O molecule and to shift the absolute potential to the NHE scale.[10, 12]

Table 1 presents the adsorption free energy at -0.5 V and adsorbed state (molecular or dissociative) for BH_4^- adsorption over the 111 (fcc) and 0001(hcp) surfaces of late transition metals. The choice of potential at which to compare adsorption energies among metals is arbitrary, as they scale equivalently with potential. We chose -0.5 V for comparison because at this potential, adsorption to Au is clearly too endergonic whereas adsorption to Pt is too exergonic. A surface offering an adsorption free energy near zero at this potential would offer a significant reduction in overpotential compared to Au(111) while potentially remaining selective against hydrolysis.

Similar to adsorption to the Pt(111) surface,[33] adsorption of the BH_4^- ion to Group VI-VIII metals is dissociative, resulting in adsorbed BH^* and $3H^*$ species. Attempts to locate a minimum energy configuration with BH_4^* in a molecular state, including constrained optimizations varying the height of the B atom above the surface and including explicit water molecules to stabilize the BH_4^* molecule, were unsuccessful. Upon exposure of these metal surfaces to the borohydride solution, the surface will likely saturate in BH^* species, and hydrogen evolution will compete with oxidation once the BH^* species are oxidized from the surface. This is in agreement with experimental borohydride oxidation tests which indicated lower selectivity and higher hydrolysis rates for platinum,[1, 7] palladium,[7] and nickel[7].

The borohydride ion adsorbs in a molecular state on the group IB metals (Au(111), Ag(111) and Cu(111)). At -0.5 V, adsorption over the Au(111) and Ag(111) surfaces is endergonic, however, the adsorption over Cu(111) is exergonic. This suggests the Cu electrodes might offer a better balance of greater activity than Au and Ag while maintaining higher selectivity against hydrolysis than Ni, Pd, and Pt.

A pure Cu electrode has been tested experimentally.[7, 34]. Though it shows activity for borohydride oxidation, the Cu electrode oxidizes at potentials near that at which borohydride is oxidized.[34-35] Therefore, pure Cu materials are not stable for use as anode electrocatalysts in borohydride fuel cells. Collectively, these results suggest that no pure metal electrocatalyst will simultaneously offer the activity, selectivity, and stability needed for use as a BOR electrocatalyst. Au-Cu binary metals are known to be more stable than pure Cu versus oxidation,[36-38] and we further consider their borohydride oxidation activity in the following section.

Table 1. Adsorption free energy (eV) of BH_4^- ions to (111) or (0001) late transition metal surfaces at -0.5 V. "D" indicates dissociative adsorption which will generate "BH+3H" on the surface; "M" indicates molecular adsorption.

	Co	Ni	Cu
	-1.25 D	-1.97 D	-0.44 M
Ru	**Rh**	**Pd**	**Ag**
-1.60 D	-1.48 D	-2.16 D	0.05 M
Os	**Ir**	**Pt**	**Au**
-1.85 D	-2.01 D	-1.85 D	0.54 M

Figure 1 presents the adsorption configuration of BH_4^* over the $Au_2Cu(111)$ surface. The Au_2Cu stoichiometry was chosen to preserve the oxidative stability with

majority Au, offer the potential for improved activity with a Cu atom included in all hollow sites, and provide a convenient ratio for our use of 3x3 unit cells. The adsorption free energy of BH_4^- is 0.32 eV at -0.5 V. This adsorption energy is 0.22 eV less endergonic than the adsorption on the pure gold surface, or stated otherwise, the free energy of adsorption will become favorable (negative) 0.22 V lower over the $Au_2Cu(111)$ surface than over the Au(111) surface. If the limiting surface reaction energies and activation barriers are similarly shifted, a 0.22 V shift in the overpotential of the BOR would be expected. Considering the total 1.64 V theoretical cell potential of the DBFC, this 0.22 V potential shift could possibly lead to a 13% improvement in the overall fuel cell efficiency relative to Au anodes. With the initial adsorption free energy encouraging, we examined the surface reaction energetics of the complete borohydride oxidation over the $Au_2Cu(111)$ catalyst surface.
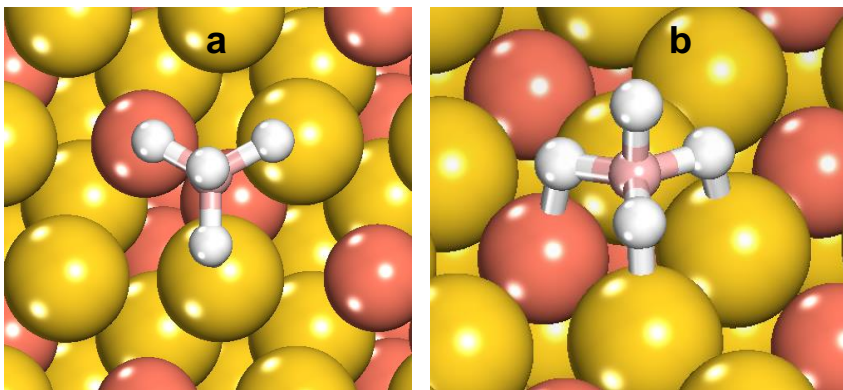
Figure 1. Adsorption configuration of BH_4^* over the $Au_2Cu(111)$ surface a) top view b) side view

*3.2. Complete borohydride oxidation mechanism over the $Au_2Cu(111)$ intermetallic surface*

3.2.1 Preferred binding site of all intermediates over the $Au_2Cu(111)$ surface

We consider optimal binding configurations and binding energies (BE) of all possible intermediates[10] of BOR over the $Au_2Cu(111)$ surface. Adsorption was considered over the high symmetry atop, bridge, fcc and hcp sites. Binding energy is calculated as the energy difference of the bound state and the total energy of the surface and gas phase species, with ZPVE and vibrational entropy corrections at 298 K included. Though the binding energy is relative to gas phase species, it is useful in identifying strongly or weakly bound species. Table 2 presents the binding energies at the optimal adsorption site and configuration over the $Au_2Cu(111)$ surface. The optimal binding configurations of intermediates are presented in Figure 2.

3.2.1.1. BH$_x$ species. BH_4^* species adsorb over the hcp (above a second layer Cu atom) hollow site with three H atoms pointing toward the surface making three B-H-M three centered, two electron hybrid bonds (BE=-2.08 eV). Similar to adsorption over the Au(111) surface, the preference for an hcp hollow site over a fcc site is minimal (-0.06 eV). The BH_4 BE to the $Au_2Cu(111)$ surface is 0.35 eV stronger than over the Au(111) surface. This leads to the 0.22 eV difference in adsorption free energy calculated with Equation 2, with the increased strength in water binding to the Au-Cu intermetallic explaining the 0.13 eV difference.

Table 2. Binding energies (BE in eV) of BOR intermediates over the $Au_2Cu(111)$ surface. Binding energies over the Au(111) surface are presented for comparison.[10]

Species	Au$_2$Cu(111) BE	Au(111) BE
BH$_4$	-2.08	-1.73
BH$_3$	-0.88	-0.55
BH$_2$	-3.13	-2.64
BH	-4.23	-4.40
B	-4.25	-4.43
BH$_3$OH	-1.28	-1.08
BH$_2$OH	-0.07	-0.06
BH$_3$O	-1.06	-0.84
BH$_2$O	-1.31	-0.93
BHOH	-2.36	-2.34
BHO	-0.61	-0.44
BOH	-2.68	-2.76
BO	-2.98	-2.85
BH(OH)$_2$	-0.04	-0.05
B(OH)$_2$	-2.21	-2.20
BHOOH	-1.72	-1.30
BOOH	-0.24	-0.23
BO$_2$	-2.36	-1.95
B(OH)$_3$	-0.05	-0.30
H	-2.25	-2.12
OH	-2.22	-1.79
H$_2$O	-0.25	-0.11
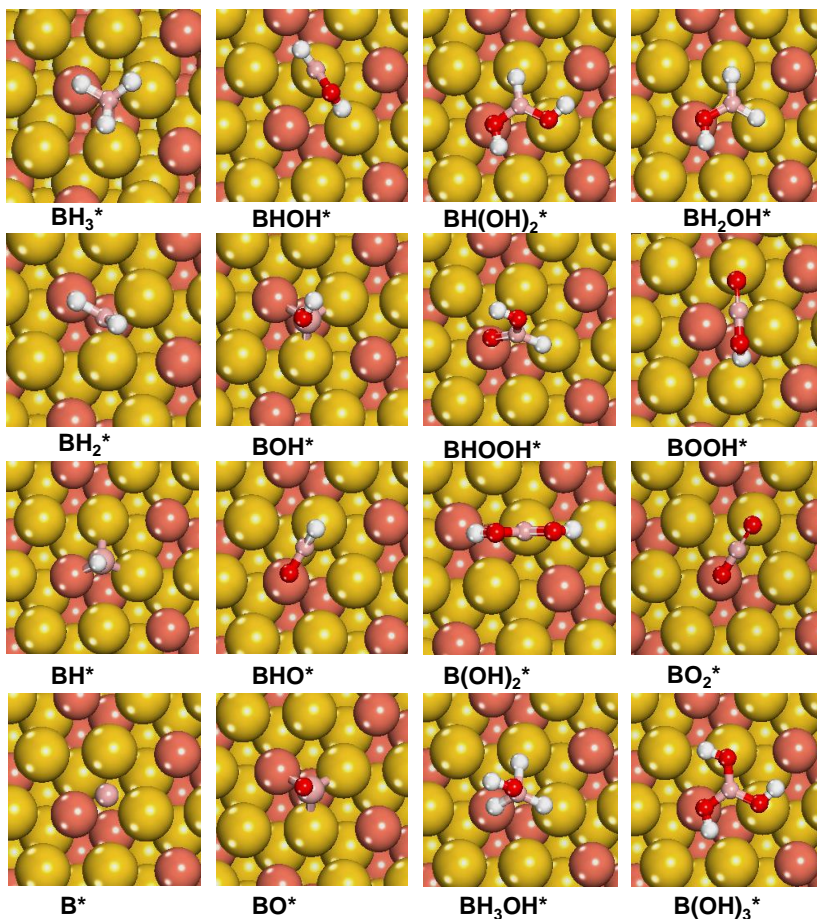
Figure 2. Optimal binding configuration of borohydride oxidation intermediates over the Au$_2$Cu(111) surface, Au=gold, Cu=mauve; H=white, B=pink, O=red.

BH$_3$ is a saturated species that binds weaker than BH$_4$ to the surface (BE=-0.88 eV), however, the binding is 0.33 eV stronger to the intermetallic than to the Au(111) surface. Stronger binding of BH$_3$ may help limit possible desorption of this partial oxidation product. BH$_2$ binds to the surface with the B atom interacting with the hollow site and one of the H atoms over the surface copper atom (BE=-3.13) and the other H atom is oriented away from the surface. The adsorption energy at the optimal binding configuration is about 0.49 eV more exothermic than to the Au(111) surface. BH* binds

to the fcc hollow site with the H atom pointing out of the surface. Binding of B atoms is slightly favored over the fcc hollow site (BE=-4.25 eV) compared to the hcp site.

3.2.1.2. BH$_x$O species. BH$_x$O species bind stronger to the intermetallic surface than the pure-Au surface. The BH$_3$OH* species adsorbs over the fcc site with two H atoms on top of Au and one H atom on top of Cu atoms (BE=-1.28 eV). The OH group points out of the surface. BH$_2$OH* is a stable gas phase species and, similar to the adsorption over the Au(111) surface, does not have a strong interaction with the surface. BH$_2$O* binds to the surface with the O atom over the Cu atop site and one of the H atoms over the Au atop site (BE=-1.31 eV). BOH* binds to the hcp hollow site with the OH group pointing away from the surface (BE=-2.68 eV). BHOH* binds to the surface with the B atom over the Au atop site (BE=-2.36 eV). The hydrogen atom in the B-H moiety points away from the surface and the H atom of the O-H bond points toward the surface. Similar to BH$_2$OH*, BHO* has a relatively weak adsorption to the surface (BE=-0.22 eV). The O atom interacts with the Cu atop site and the B atom is over the Au atop site. Similar to BOH*, BO* binds to the surface with the B over the hcp hollow site and O pointing away from the surface (BE=-2.98).

BH$_x$O$_2$ species. BH(OH)$_2$* is a stable gas phase species and, similar to binding to the Au(111) surface, does not bind strongly to the Au$_2$Cu(111) surface. B(OH)$_2$* binds strongly to the Au atop site with the H atoms pointing toward the nearby Au and Cu atop sites (BE=-2.21 eV). BHOOH* binds to the surface with the O atom on the Cu atop site, the H atom on the Au atop site and OH group points away from the surface(BE=-1.72 eV). BOOH* is a stable species that binds weakly to the Au$_2$Cu(111) surface (BE=-0.24 eV). BO$_2$* binds with one O atom on the Cu atop site, the other O atom on the Au atop

site. The B atom resides over the bridge site (BE=-2.36 eV). BO_2^* binding to the Au_2Cu (111) surface is 0.41 eV stronger than to the Au(111) surface.

3.2.2. Elementary oxidation energetics of BH_4^* oxidation over the $Au_2Cu_1(111)$ surface

The DFT energies of surface bound intermediates can be used to construct a reaction free energy diagram. For a general oxidation reaction converting adsorbed reactant R* to adsorbed oxidized product O*, the reaction and reaction free energy are written as:

$$R^* + xOH_{aq}^- \rightarrow O^* + yH_2O_{aq} + ne^- \qquad (3)$$
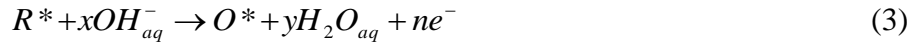
$$\Delta G_{rxn} = G_{O^*} - neU + yG_{H_2O_{aq}} - G_{R^*} - xG_{OH_{aq}^-} \qquad (4)$$

Equations 3 and 4 may represent either an elementary step or a collection of elementary steps, and combined with equation 2 can be used to construct a reaction energy free energy diagram with all states referenced to the initial aqueous borohydride ion. This approach was previously applied to construct reaction free energy diagrams for borohydride oxidation over the Au(111) and Pt(111) surfaces [10-11].

The reaction energy diagram for borohydride oxidation over $Au_2Cu(111)$ is illustrated in Figure 3 at an electrode potential of -0.45 V. The initial adsorption free energy of the BH_4^- ion at -0.45 V over the $Au_2Cu_1(111)$ surface is equivalent to the value for the Au(111) surface at -0.23 V.[10] All the following oxidation reaction energies are exergonic and, therefore, favorable at this potential. Considering only the species along the minimum energy oxidation path, on average each species is 0.13 eV more stable on the $Au_2Cu(111)$ surface than on the Au(111) surface.
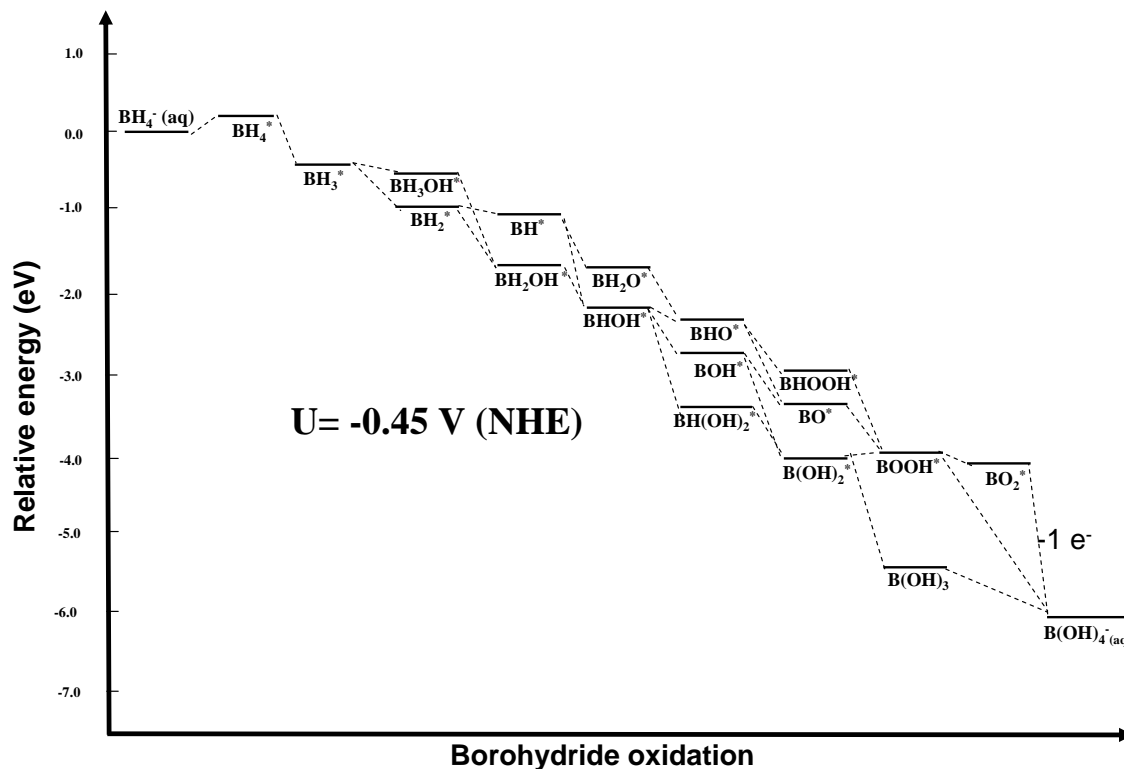
Figure 3. Reaction energy diagram for borohydride oxidation over the $Au_2Cu_1(111)$ surface at -0.45 V. Each step to the right indicates a 1e$^-$ oxidation step with the exception of the final product desorption step. Hydroxide ion reactants and water molecule products are left off the diagram for clarity. Dashed lines represent plausible elementary reactions. Conditions for free energy calculations: $[BH_4^-]$=0.03 M, $[OH^-]$=2 M, T=298 K

3.3. Activation barriers for dehydrogenation of BH_4^*

The activation barriers for elementary surface reactions are not included in Figure 3. The activation energy corresponding to the first step of the mechanism of borohydride oxidation, the dehydrogenation of BH_4^* to BH_3^* (reaction 5) over $Au_2Cu_1(111)$, is presented in this section:

$$BH_4^* \rightarrow BH_3^* + H^* \qquad\qquad (5)$$

Figure 4 illustrates the most favorable adsorption configuration of reactant (a), intermediate of reaction (b) and products (c). The activation barrier for the lowest energy path of this reaction is 0.49 eV, which is 0.12 eV higher than that obtained on Au(111)

18

[1]. The transition state was confirmed to have a single imaginary harmonic oscillator frequency of -262.7 cm^{-1}.

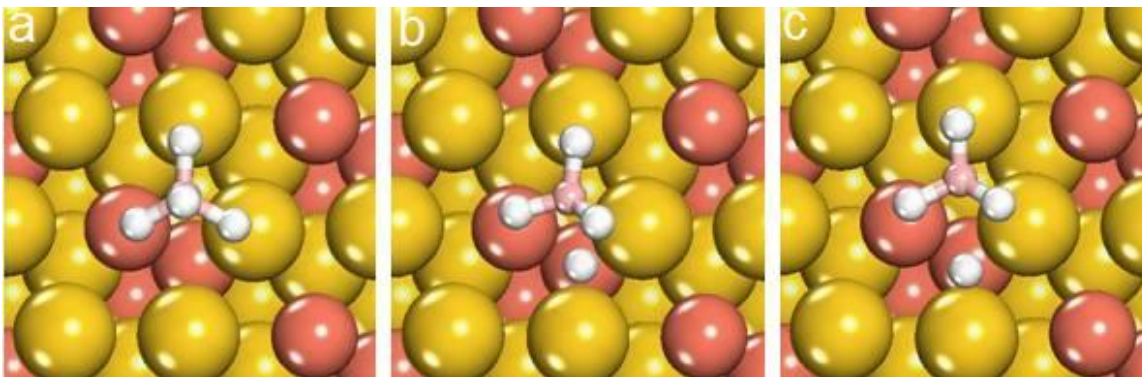Figure 4. (a) Initial state, (b) transition state and (c) final state of the dehydrogenation of BH_4^* to BH_3^* over Au_2Cu_1 (111) surface.

A higher barrier of the first reaction step on $Au_2Cu(111)$ is a result of more stable initial state and shorter reaction coordinate for this reaction compared to the Au(111) surface. Though the activation barrier referenced to the initial state is higher over the $Au_2Cu(111)$ surface than the Au(1111) surface, the barrier is lower by 0.10 eV on the bimetallic compared to the pure Au surface when the transition state is referenced to the non-bound BH_4^- state. As the initial BH_4^- adsorption is uphill in free energy at potentials of interest, the barrier relative to the non-bound state is kinetically relevant (ie, BH_4^* coverage is low), and the intermetallic surface will offer more rapid initial activation of borohyride than the pure Au(111) surface.

3.4. Activation barriers for dehydrogenation of BH_3^*

19

The adsorption energy corresponding to the second step of the mechanism of borohydride oxidation, the dehydrogenation of BH_3^* to BH_2^* (reaction 6) over $Au_2Cu_1(111)$, is discussed in this section:

$$BH_3^* \rightarrow BH_2^* + H^* \qquad\qquad (6)$$

BH_3^* has been identified as a stable reaction intermediate for the BOR reaction.[11] Figure 5 illustrates the most favorable adsorption configuration of reactant (a), intermediate of reaction (b) and products (c). The activation barrier for this reaction was 0.42 eV, which is 0.39 eV lower than that obtained on Au(111) [1]. The transition state was confirmed to have a single imaginary harmonic oscillator frequency of -541 cm^{-1}.
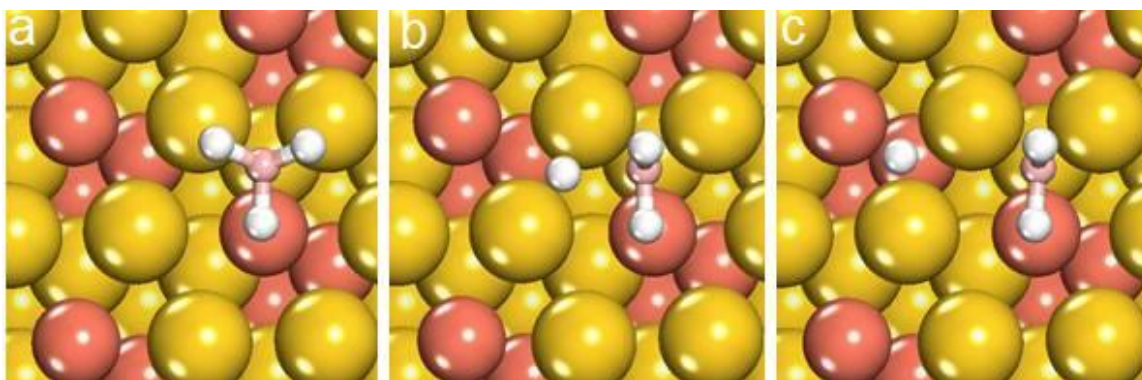

Figure 5. (a) Initial state, (b) transition state and (c) final state of the dehydrogenation of BH_3^* to BH_2^* over Au_2Cu_1 (111) surface.

3.5. Activation barriers for dehydrogenation of BH_2OH^*

BH_2OH^* species are have been identified as the most stable reaction intermediate for borohydride oxidation over the Au(111) surface.[11] The activation energy corresponding to BH_2OH^* dehydrogenation (reaction 7) over $Au_2Cu_1(111)$, is discussed in this section:

$$BH_2OH^* \rightarrow BHOH^* + H^* \qquad\qquad (7)$$

Figure 6 illustrates the most favorable adsorption configuration of reactant (a), intermediate of reaction (b) and products (c). The activation barrier for this reaction was 0.39 eV, which is 0.67 eV lower than that obtained on Au(111) [1]. The transition state was confirmed to have a single imaginary harmonic oscillator frequency of -359 cm^{-1}.
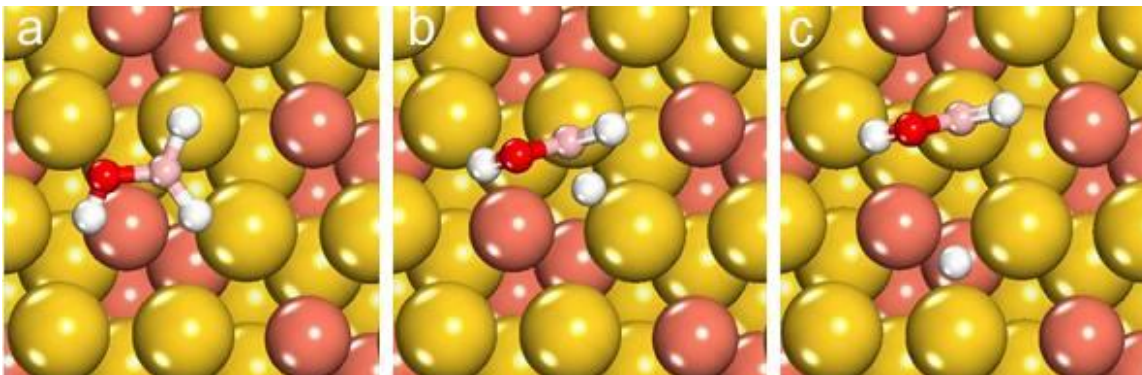

Figure 6. (a) Initial state, (b) transition state and (c) final state of the dehydrogenation of BH$_2$OH* to BHOH* over Au$_2$Cu$_1$ (111) surface.

3.6. Potential dependence of activation barriers

The dehydrogenation barriers presented in the previous sections can be converted to potential dependent, electrochemical barriers using the method we have previously developed .[11, 39] For example, the barrier for the electrochemical reaction,

$$BH_4*+OH_{aq}^- \rightarrow BH_3*+H_2O_{aq}+e^- \qquad (8)$$
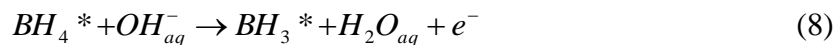
is approximated using equation 9:

$$Ea(U)=Ea^0-\beta(U-U_0) \qquad (9)$$

where Ea^0 is the activation barrier of the chemical step, β is the symmetry factor and U_0 is the equilibrium potential for surface hydrogen oxidation.

For the Au(111) surface, we previously determined U_0 and a β value that allowed a DFT-based microkinetic model to match experimental kinetics,[11] such that

$$Ea(V) = Ea^0 - 0.44(U + 1.19) \qquad (10)$$

The calculated value for U_0 on $Au_2Cu1(111)$ surface is -1.03 V(NHE). Therefore, the activation barriers for electro-oxidation reactions over the Au2Cu1(111) surface is

$$Ea(V) = Ea^0 - 0.44(U + 1.03) \qquad (11)$$

where we presume an equivalent symmetry factor on the intermetallic surface. Initial electrocatalytic conversion of BH_4^* (reaction 8) has a barrier, referenced to the solution phase BH_4^- ion, of 0.61 eV over the Au(111) surface at -0.5 V(NHE). The equivalent barrier on the $Au_2Cu1(111)$ surface is 0.58 eV at -0.5 V(NHE), suggesting faster borohydride activation on the intermetallic. Similarly, the barrier for the electrochemical oxidation of BH_3 on $Au_2Cu(111)$ at -0.5 V(NHE) is 0.19 eV, 0.32 eV lower than on the Au(111) surface. For BH_2OH oxidation, the $Au_2Cu(111)$ barrier of 0.16 eV at -0.5 V(NHE) is 0.6 eV less than the barrier on Au(111). The intermetallic is clearly significantly more active for the rate limiting B-H bond activation steps than the Au(111), suggesting it will produce more rapid borohydride oxidation kinetics.

3.7. Experimental evaluation of Au-Cu alloys for borohydride electrooxidation

To realize the DFT predicted improved BOR performance of AuCu binary metal catalysts compared to a pure Au catalyst, we synthesized, characterized, and tested AuCu electrodes. Electrodeposition was used to prepare a AuCu film for electrokinetic testing. Prior to electrokinetic testing, X-ray diffraction (XRD) and energy dispersive x-ray spectroscopy (EDS) were used to characterize the film.

3.7.1. Deposited Au-Cu sample characterization with XRD and EDS

Figure 7 shows the X-ray diffraction results for a Au-Cu sample electrodeposited

from a 1mM $HAuCl_4$ and 2mM $CuSO_4$ solution. Two peaks are identified in the X-ray
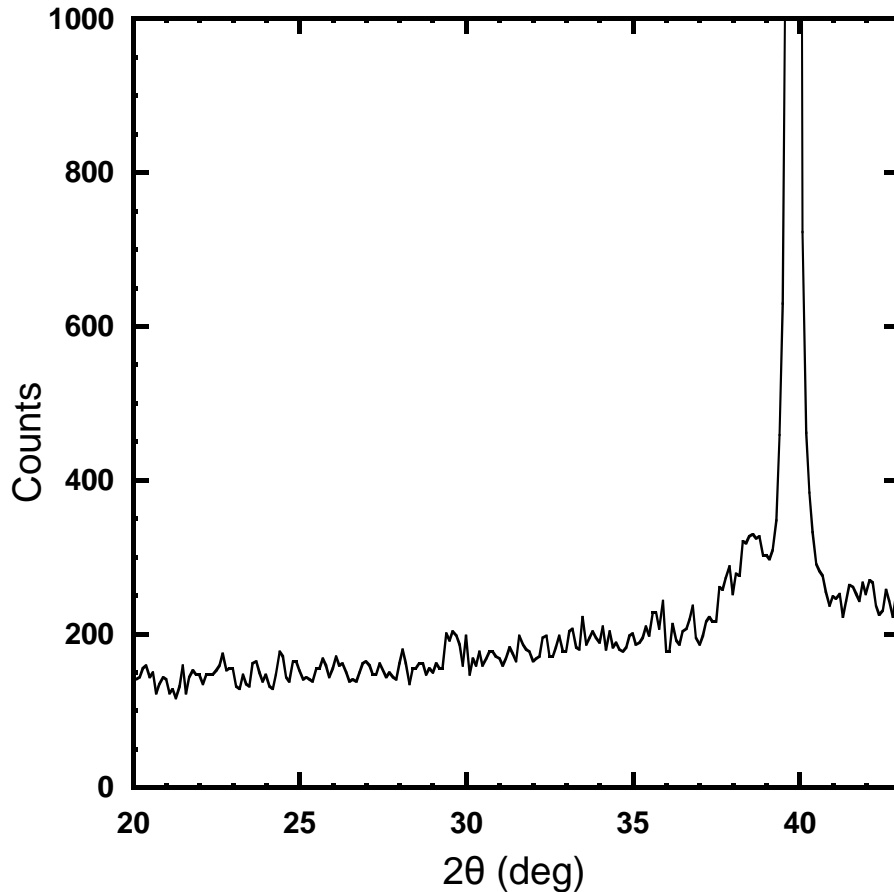

Figure 7. X-ray diffraction results for Au-Cu sample deposited from a solution of 1 mM $HAuCl_4$ and 2 mM $CuSO_4$.

pattern. The large peak indexes to the Pt(111) peak of the substrate electrode. A second

peak identified at a 2θ of 38.592 corresponds to the electrodeposited AuCu(111) with a

spacing of d=2.33 Å using Bragg's law. The assignment of this peak to the AuCu film

was confirmed by varying the concentration of Cu precursor for electrodeposition such

that a 100% Au (Figure 8) and a 90% Cu sample (not shown) were also prepared. The

minor (111) peak was repeatable across multiple deposition experiments following the
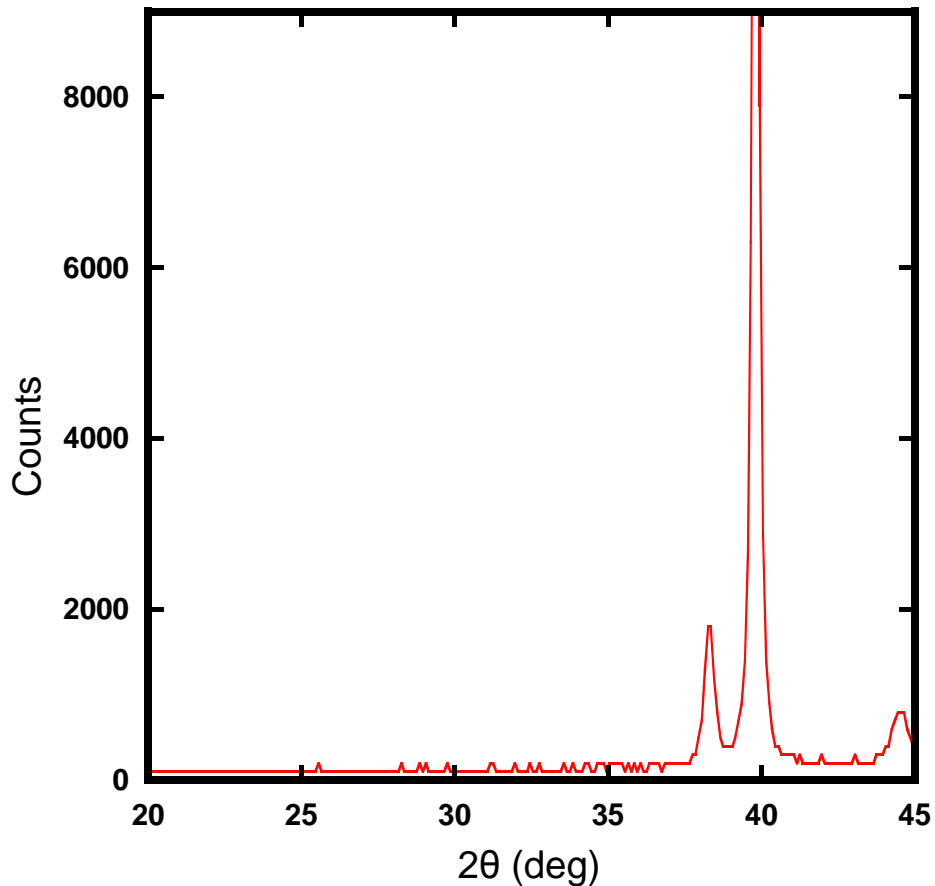
same protocol and does

Figure 8. X-ray diffraction results for pure Au sample deposited from a solution of 3 mM
$HAuCl_4$

not exist on the pure platinum diffraction pattern. This minor peak corresponds to a Au-

Cu(111) surface with a lattice constant of 4.036 Å. Based on the lattice constant the

deposited film is 11.5% Cu and 88.5% Au, as calibrated by a continuous curve derived

from empirical potentials that fits well to experimentally measured lattice constants.[32]

A sample of Au-Cu deposited alloy from a solution of 1mM $HAuCl_4$ and 5mM $CuSO_4$ was confirmed by X-ray diffraction to have more than 60% copper which is not appropriate for DBFC application due to facile Cu oxidation. Though deposition of a 33% Cu sample was desired, the composition of a sample deposited from a solution of 1mM $HAuCl_4$ and 3 mM $CuSO_4$ was not possible to identify with XRD due to the integration of the Au-Cu peak into the Pt(111) peak.

EDS was further used to confirm the presence and relative magnitudes of Au and Cu in the deposited films. Though quantitative analysis of the compositions was not attempted, EDS demonstrated that relative copper to gold peak areas increase with increasing copper precursor concentration in the deposition solution and is consistent with compositions determined by XRD experiments.

3.7.2. Linear sweep voltammetry of borohydride oxidation of the Au-Cu binary metal

Figure 9 shows the linear sweep voltammogram of pure copper deposited over the platinum substrate in a 2 M NaOH solution, without $NaBH_4$ added. Only a small oxidation peak is observed at -0.26 V(NHE), corresponding to the oxidation of the copper surface. Alternatively, the large oxidation peak at approximately 0 V likely corresponds to the bulk oxidation and dissolution of the copper surface.[40] Figure 10 presents the experimental linear sweep voltammetry results for the $Au_{88.5}Cu_{11.5}$ binary metal compared to a pure Au electrode. The borohydride oxidation peak for the Au electrode is at -0.16 V, whereas for the $Au_{88.5}Cu_{11.5}$ surface two oxidation peaks are observed. The first oxidation peak at -0.33 V(NHE) (Figure 10) for the $Au_{88.5}Cu_{11.5}$ electrode cannot be assigned to copper oxidation, and is instead assigned to the borohydride oxidation peak

over the $Au_{88.5}Cu_{11.5}$ electrode. The second oxidation peak for the binary metal sample, at -0.01 V(NHE), likely represents a mixed effect of borohydride oxidation and copper oxidation over the electrode surface. The $Au_{88.5}Cu_{11.5}$ electrode decreases the borohydride oxidation overpotential by 0.17 V. The same value of 0.17 V is measured peak to peak and at a current of 2 mA, suggested the difference does not arise from mass transfer differences between the two electrodes. The 0.17 V shift would correspond to a 10 % increase in the overall

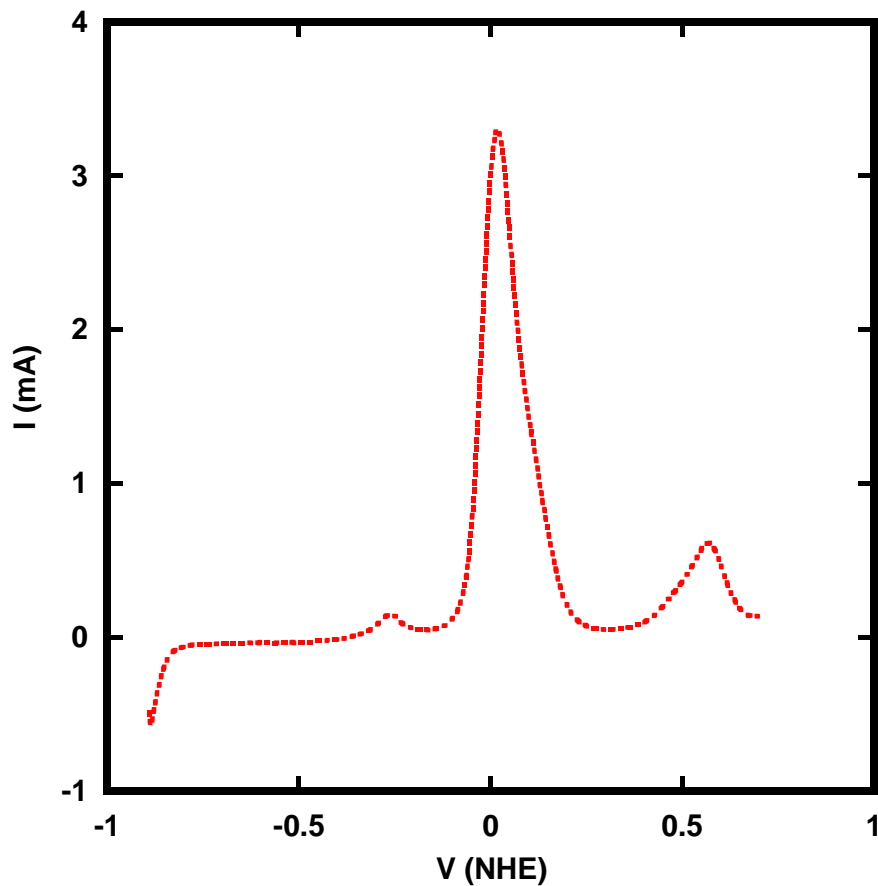Figure 9. Linear sweep voltammogram of deposited pure copper in 2 M NaOH solution. Scan Rate= 25 mVs^{-1}, Electrode diameter= 5 mm, T = 298 K.
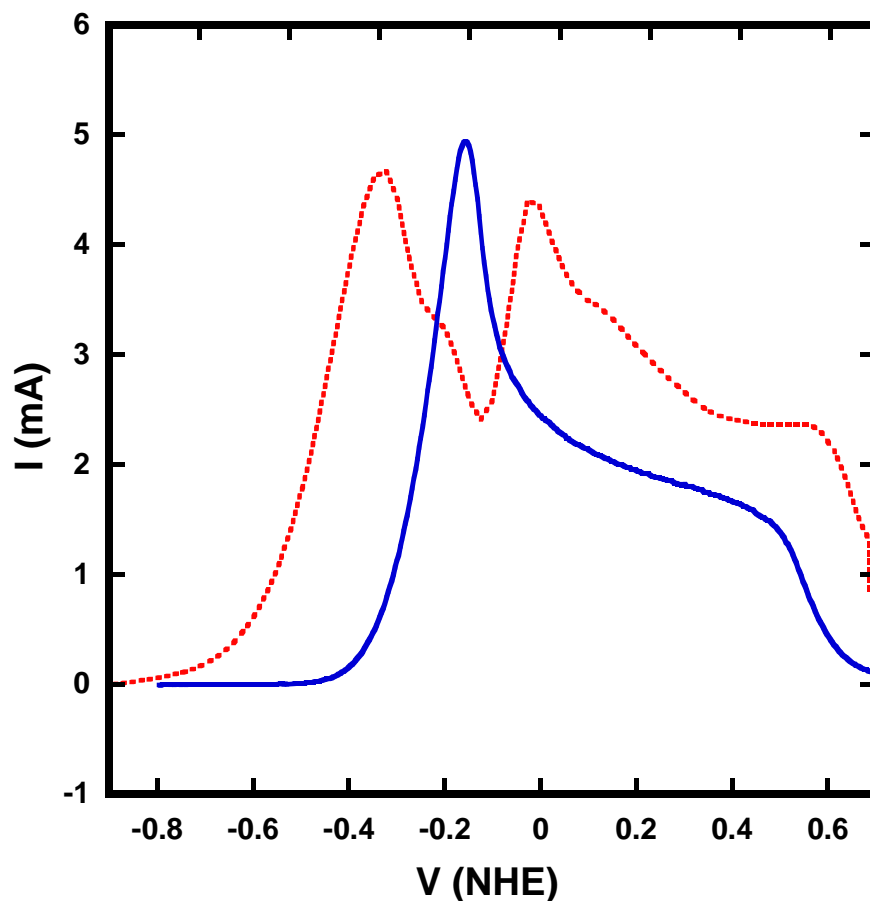
Figure 10. Borohydride oxidation over the $Au_{88.5}Cu_{11.5}$ surface (dashed red) compared to the pure gold electrode (solid blue). Electrode diameter in both cases 5 mm, scan rate =25 mVs^{-1}, $[BH_4^-]$=0.03 M, $[OH^-]$=2 M, T= 298 K

fuel cell efficiency, and is similar to the predicted shift based on DFT calculations for the $Au_2Cu_1(111)$ surface.   However, the binary metal electrodes are not as oxidatively stable as a pure gold electrode, and their use would be limited to potentials lower than -0.2 V to avoid catalyst oxidation in the high pH condition.

These results agree with that reported by Yi et al.,[41] who deposited Au-Cu nanoparticles at different proportions (Au/C, $Au_{75}Cu_{25}$/C, $Au_{67}Cu_{33}$/C, $Au_{50}Cu_{50}$/C) on Carbon Vulcan and carried out cyclic voltammetry, chronopotentiometry and

chronoamperometry for borohydride oxidation. The authors conclude that the optimum proportion of Au and Cu for borohydride oxidation was $Au_{67}Cu_{33}$, obtaining a current density 46% larger than using pure Au/C. An overpotential of -0.70 V was measured when $Au_{67}Cu_{33}$/C was used compared to -0.57 V on Au/C, improving the performance of the DBFC from 19.9 mW cm^{-2} using Au/C as the anode material to 51 mW cm^{-2} using $Au_{67}Cu_{33}$.

3.8. Computational screening of borohydride adsorption over other surface alloys

The AuCu binary metal BOR catalyst was arrived at based on a rationale of adding Cu to Au improve activity while providing more oxidative stability than pure Cu. Similarly, we might expect binary compositions of group VIII and IB metals to balance the BH_4 affinity and B-H dissociation activity for a balance between activity and selectivity to direct oxidation. To explore the potential of other binary metal surfaces for improving the performance of BOR anodes, the borohydride ion adsorption free energy was evaluated. Strong dissociative adsorption is indicative of a very active catalyst, which is expected to produce to large amount of hydrogen and less than 8 e$^-$ per BH_4^- ion converted. Metal/alloy surfaces with mild molecular adsorption at potentials between -0.5 to -0.7 V could offer more activity while maintaining selectivity for the BOR. Table 3 presents the binding energy and adsorption free energy at -0.5 V(NHE) of the BH_4^- ion over a series of VIII-IIB binary metal surfaces. Binary metals reported in Table 3 are surface alloys only and are not bulk intermetallic alloys. Using the Ag_2Ni surface alloy as an example, a 4 layer slab is used in calculations. The first 3 layers are all Ag atoms,

whereas the surface layer consists of 6 Ag atoms and 3 Ni atoms evenly distributed in the 3x3 cell.

Table 3. BH_4 binding energies and BH_4^- ion adsorption free energies at -0.5 V over Group VIII-IB binary metal (111) and (0001) surfaces (eV). The adsorption free energies to the pure Au and the Au_2Cu_1 intermetallic are reported for reference.

Surface alloy	Ag_2Ni	Ag_2Pd	Ag_2Pt	Ag_2Rh	Ag_2Ru	Au_2Ni	Au_2Pd	Au_2Pt	Au_2Rh	Au_2Ru	Au	Au_2Cu
Binding energy (eV)	-2.88	-2.55	-2.58	-2.64	-2.7	-2.66	-2.13	-2.22	-2.34	-2.35	-1.73	-2.08
Adsorption energy (eV)	-0.39	-0.17	-0.24	-0.2	-0.06	0.06	0.3	0.13	0.2	0.41	0.54	0.32

Binding of borohydride species is stronger on all of these surfaces compared to the Au(111) surface, suggesting any of the surface alloys could be more active than a pure Au electrode. All of these surfaces allow for binding energies intermediate of the less active Au(111) surface and the non-selective Pt(111) surface, indicating a potential improvement in both activity and selectivity for the BOR in comparison with the pure metal surfaces. The adsorption to each of these surfaces may be classified as molecular, although the B-H bond over the Group VIII metal atom extends upon adsorption. For example, for the Au_2Pt surface alloy, the lengths of B-H bonds for the H atoms that interact with gold atop sites are 1.25 Å, whereas the bond length extends to 1.38 Å for the B-H bond with the H over the Pt atop site. This partial B-H bond dissociation may indicate a tendency towards non-selective hydrolysis reactions, however, further mechanistic study would be needed and examination of the H recombination rate on the binary metal surface would merit consideration.

4. Conclusions

AuCu alloys are proposed as an alternative catalyst for borohydride direct oxidation based on DFT calculations and experimental linear sweep voltammetry results. Our DFT model predicts less endothermic adsorption of the BH_4^- ion, stronger binding of reaction intermediates to the $Au_2Cu_1(111)$ surface and, lower overall activation barrier in comparison to the Au(111) surface. This suggests that AuCu binary electrodes are more active than Au electrodes for borohydride anodic oxidation. Alternatively, due to the molecular adsorption of the BH_4^* species over the catalyst binary metal surface, these electrodes could be as selective to complete oxidation as gold electrodes. A Au-Cu electrode was prepared using electrodeposition techniques and tested by linear sweep voltammetry experiments. At high concentrations of copper on the surface, surface oxidation prevents borohydride oxidation. At the composition of 11.5% Cu, 88.5% Au, the BOR catalyst activity increased, indicated by a 0.17 V decrease in the anodic overpotential. This experimental result realized the predicted overpotential reduction from DFT calculation. This first-principles guided design demonstrates the use of theory to guide electrocatalyst design, beginning with mechanism determination and determination of key predictor energetics through rational evaluation of binary metal compositions and experimental realization of predicted improvements. A series of binary metal compositions were suggested that may offer improved BOR performance based on DFT results.

Acknowledgements

References

1.   Gyenge, E., Electrooxidation of borohydride on platinum and gold electrodes: implications for direct borohydride fuel cells. *Electrochim. Acta* **2004,** *49*, 965-978.

2.   Mirkin, M. V.; Yang, H.; Bard, A. J., Borohydride Oxidation at a Gold Electrode. *J. Electrochem. Soc.* **1992,** *139*, 2212-2217.

3.   Chatenet, M.; Micoud, F.; Roche, I.; Chainet, E., Kinetics of sodium borohydride direct oxidation and oxygen reduction in sodium hydroxide electrolyte - Part I. BH4-electro-oxidation on Au and Ag catalysts. *Electrochim. Acta* **2006,** *51* (25), 5459-5467.

4.   Chatenet, M.; Lima, F. H. B.; Ticianelli, E. A., Gold is not a Faradaic-Efficient Borohydride Oxidation Electrocatalyst: An Online Electrochemical Mass Spectrometry Study. *J. Electrochem. Soc.* **2010,** *157* (5), B697-B704.

5.   Finkelstein, D. A.; Da Mota, N.; Cohen, J. L.; Abruna, H. D., Rotating Disk Electrode (RDE) Investigation of BH4- and BH3OH- Electro-oxidation at Pt and An: Implications for BH4- Fuel Cells. *J. Phys. Chem. C* **2009,** *113* (45), 19700-19712.

6.   Sanli, E.; Celikkan, H.; Uysal, B. Z.; Aksu, M. L., Anodic behavior of Ag metal electrode in direct borohydride fuel cells. *International Journal of Hydrogen Energy* **2006,** *31*, 1920-1924.

7.   Liu, B. H.; Li, Z. P.; Suda, S., Electrocatalysts for the anodic oxidation of borohydrides. *Electrochim. Acta* **2004,** *49*, 3097-3105.

8.   Cheng, H.; Scott, K.; Lovell, K., Material Aspects of the Design and Operation of Direct Borohydride Fuel Cells. *Fuel Cells* **2006,** *5*, 367-375.

9.   Liu, B. H.; Li, Z. P.; Suda, S., Anodic Oxidation of Alkali Borohydrides Catalyzed by Nickel. *J. Electrochem. Soc.* **2003,** *150*, A398-A402.

10.   Rostamikia, G.; Janik, M. J., Borohydride Oxidation over Au(111): A First-Principles Mechanistic Study Relevant to Direct Borohydride Fuel Cells. *J. Electrochem. Soc.* **2009,** *156*, B86-B92.

11.   Rostamikia, G.; Mendoza, A. J.; Hickner, M. A.; Janik, M. J., First-principles based microkinetic modeling of borohydride oxidation on a Au(111) electrode. *J. Power Sources* **2011,** *196*, 9228-9237.

12.   Rostamikia, G.; Janik, M. J., First Principles Mechanistic Study of Borohydride Oxidation over the Pt(111) Surface. *Electrochim. Acta* **2010,** *55*, 1175-1183.

13.   Merino-Jimenez, I.; Janik, M. J.; de Leon, C. P.; Walsh, F. C., Pd-Ir alloy as an anode material for borohydride oxidation. *J. Power Sources* **2014,** *269*, 498-508.

14.   Atwan, M. H.; Macdonald, C. L. B.; Northwood, D. O.; Gyenge, E. L., Colloidal Au and Au-alloy catalysts for direct borohydride fuel cells: Electrocatalysis and fuel cell performance. *J. Power Sources* **2006,** *158*, 36-44.

15.   Gyenge, E.; Atwan, M.; Northwood, D., Electrocatalysis of Borohydride Oxidation on Colloidal Pt and Pt-Alloys (Pt-Ir, Pt-Ni, and Pt-Au) and Application for Direct Borohydride Fuel Cell Anodes. *J. Electrochem. Soc.* **2006,** *153*, A150-A158.

16.   Atwan, M. H.; Northwood, D. O.; Gyenge, E. L., Evaluation of colloidal Ag and Ag-alloys as anode electrocatalysts for direct borohyride fuel cells. *International Journal of Hydrogen Energy* **2007,** *32*, 3116-3125.

17.   Simoes, M.; Baranton, S.; Coutanceau, C., Electrooxidation of Sodium Borohydride at Pd, An, and PdxAu1-x Carbon-Supported Nanocatalysts. *J. Phys. Chem. C* **2009,** *113* (30), 13369-13376.

18.   He, P.; Wang, Y.; Wang, X.; Pei, F.; Wang, H.; Liu, L.; Yi, L., Investigation of carbon supported Au–Ni bimetallic nanoparticles as electrocatalyst for direct borohydride fuel cell. *J. Power Sources* **2011,** *196* (3), 1042-1047.

19.   Šljukić, B.; Milikić, J.; Santos, D. M. F.; Sequeira, C. A. C.; Macciò, D.; Saccone, A., Electrocatalytic performance of Pt–Dy alloys for direct borohydride fuel cells. *J. Power Sources* **2014,** *272*, 335-343.

20.   Olu, P.-Y.; Job, N.; Chatenet, M., Evaluation of anode (electro)catalytic materials for the direct borohydride fuel cell: Methods and benchmarks. *J. Power Sources* **2016,** *327*, 235-257.

21.   Behmenyar, G.; Akın, A. N., Investigation of carbon supported Pd–Cu nanoparticles as anode catalysts for direct borohydride fuel cell. *J. Power Sources* **2014,** *249*, 239-246.

22.   Li, S.; Wang, L.; Chu, J.; Zhu, H.; Chen, Y.; Liu, Y., Investigation of Au@Co-B nanoparticles as anode catalyst for direct borohydride fuel cells. *International Journal of Hydrogen Energy* **2016,** *41* (20), 8583-8588.

23.   He, P.; Wang, X.; Liu, Y.; Liu, X.; Yi, L., Comparison of electrocatalytic activity of carbon-supported Au–M (M = Fe, Co, Ni, Cu and Zn) bimetallic nanoparticles for direct borohydride fuel cells. *International Journal of Hydrogen Energy* **2012,** *37* (16), 11984-11993.

24.   Arevalo, R. L.; Escaño, M. C. S.; Kasai, H., Mechanistic Insight into the Au-3d Metal Alloy-Catalyzed Borohydride Electro-Oxidation: From Electronic Properties to Thermodynamics. *ACS Catalysis* **2013,** *3* (12), 3031-3040.

25.   Arevalo, R. L.; Escano, M. C. S.; Wang, A. Y.-S.; Kasai, H., Structure and stability of borohydride on Au(111) and Au3M(111) (M = Cr, Mn, Fe, Co, Ni) surfaces. *Dalton Trans.* **2013,** *42* (3), 770-775.

26.   Kresse, G.; Hafner, J., *Ab initio* molecular dynamics for liquid metals. *Phys. Rev. B* **1993,** *47* (1), 558-561.

27.   Kresse, G.; Furthmuller, J., Efficiency of ab-initio total energy calculations for metals and semiconductors using a plane-wave basis set. *Computational Materials Science* **1996,** *6*, 15-50.

28.   Kresse, G.; Furthmuller, J., Efficient iterative schemes for *ab initio* total-energy calculations using a plane wave basis set. *Phys. Rev. B* **1996,** *54* (16), 11169-11186.

29.   Kresse, G.; Joubert, D., From ultrasoft pseudopotentials to the projector augmented-wave method. *Phys. Rev. B* **1999,** *59* (3), 1758-1775.

30.   Perdew, J. P.; Chevary, J. A.; Vosko, S. H.; Jackson, K. A.; Pederson, M. R.; Singh, D. J.; Fiolhais, C., Atoms, molecules, solids, and surfaces: Applications of the generalized gradient approximation for exchange and correlation. *Phys. Rev. B* **1992,** *46* (11), 6671-7895.

31.   Monkhorst, H. J.; Pack, J. D., SPECIAL POINTS FOR BRILLOUIN-ZONE INTEGRATIONS. *Phys. Rev. B* **1976,** *13* (12), 5188-5192.

32.   Ackland, G. J.; Vitek, V., MANY-BODY POTENTIALS AND ATOMIC-SCALE RELAXATIONS IN NOBLE-METAL ALLOYS. *Phys. Rev. B* **1990,** *41* (15), 10324-10333.

33.   Rostamikia, G.; Janik, M. J., Direct borohydride oxidation: mechanism determination and design of alloy catalysts guided by density functional theory. *Energy & Environmental Science* **2010,** *3* (9), 1262-1274.

34.   Duan, D. H.; Zhao, Y. F.; Liu, S. B.; Wu, A. L., Electrochemical Oxidation of Borohydride on Cu Electrode. *Adv. Mater. Res.* **2012,** *347-353*, 3264-3267.

35.   Pourbaix, M., *Atlas of Electrochemical Equilibria in Aqueous Solutions*. NACE: Houston, TX, 1974.

36.   Ateya, B. G.; Geh, G.; Carim, A. H.; Pickering, H. W., Selective Dissolution below the Critical Potential and Back Alloying in Copper-Gold Alloy. *J. Electrochem. Soc.* **2002,** *149*, B27-B33.

37.   Duffo, G. S.; Farina, S. B.; Galvele, J. R., Stress corrosion cracking of 18 carat gold. *Corros. Sci.* **2004,** *46*, 1-4.

38.   Fritz, J. D.; Pickering, H. W., Selective Anodic Dissolution of Cu-Au Alloys: TEM and Current Transient Study. *J. Electrochem. Soc.* **1991,** *138*, 3209-3218.

39.   Nie, X. W.; Esopi, M. R.; Janik, M. J.; Asthagiri, A., Selectivity of CO2 Reduction on Copper Electrodes: The Role of the Kinetics of Elementary Steps. *Angewandte Chemie-International Edition* **2013,** *52* (9), 2459-2462.

40.   Kang, M. C.; Gewirth, A. A., Voltammetric and force spectroscopic examination of oxide formation on Cu(111) in basic solution. *J. Phys. Chem. B* **2002,** *106* (47), 12211-12220.

41.   Yi, L.; Song, Y.; Liu, X.; Wang, X.; Zou, G.; He, P.; Yi, W., High activity of Au–Cu/C electrocatalyst as anodic catalyst for direct borohydride-hydrogen peroxide fuel cell. *International Journal of Hydrogen Energy* **2011,** *36* (24), 15775-15782.